Confirmation of the Shears Mechanism in Near-Spherical Tin Nuclei

D. G. Jenkins,[1] R. Wadsworth,[1] J. A. Cameron,[2] R. M. Clark,[3] D. B. Fossan,[4] I. M. Hibbert,[1,*] V. P. Janzen,[5] R. Krücken,[3,†] G. J. Lane,[4,‡] I. Y. Lee,[3] A. O. Macchiavelli,[3] C. M. Parry,[1] J. M. Sears,[4] J. F. Smith,[4,§] and S. Frauendorf[6,‖]

[1]*Department of Physics, University of York, Heslington, York Y01 5DD, United Kingdom*
[2]*Department of Physics and Astronomy, McMaster University, Hamilton, Ontario, Canada L85 4M1*
[3]*Lawrence Berkeley National Laboratory, Berkeley, California 94720*
[4]*Department of Physics, State University of New York at Stony Brook, Stony Brook, New York 11794-3800*
[5]*Chalk River Laboratories, AECL Research, Chalk River, Ontario, Canada K0J 1J0*
[6]*FZ Rossendorf, Postfach 510119, D-01314 Dresden, Germany*

(Received 2 February 1999)

Lifetimes of states of a magnetic dipole band in each of the nuclei ^{106,108}Sn have been obtained using the Doppler shift attenuation method. The deduced $B(M1)$ transition rates show the characteristic behavior associated with the shears mechanism. A simplified semiclassical analysis yields $B(M1)$ values in qualitative agreement with those expected for previously assigned configurations. The results suggest extremely low deformations for these dipole structures. In particular, the ^{106}Sn band appears to be the first example of almost pure magnetic rotation in a spherical nucleus.

PACS numbers: 21.10.Tg, 23.20.Lv, 25.70.Gh, 27.60.+j

Considerable evidence has now been collated for the existence of "rotational-like" magnetic dipole ($M1$) bands in the lead and tin regions (e.g., [1–3]). It has been proposed that the mechanism responsible for the existence of such structures in weakly deformed nuclei is the shears mechanism [4]. This mechanism is so called by analogy with the closing of a pair of shears since nearly all the angular momentum is generated by the gradual alignment of proton and neutron spin vectors ($\underline{\mathbf{j}}_\pi$ and $\underline{\mathbf{j}}_\nu$), which are initially coupled perpendicularly at the bandhead, with the total angular momentum vector, $\underline{\mathbf{I}}$ (Fig. 1). This behavior has been discussed in terms of the tilted axis cranking (TAC) model [4–6] and the configurations and properties of the observed bands have been described, with some success, within the model [1,3]. The model introduces a new form of quantized rotation, "magnetic rotation" [4], where the rotational symmetry breaking arises from the anisotropic arrangement of nucleon currents. A more phenomenological description of the shears mechanism has recently been presented in terms of the coupling of two long vectors, $\underline{\mathbf{j}}_\nu$ and $\underline{\mathbf{j}}_\pi$ [7,8]. Their interaction is mediated by an effective quadrupole force attributed to particle-vibration coupling. Both this and the TAC model predict a definitive signature characteristic of the shears mechanism, namely, that the $B(M1)$ transition rates between the levels in the bands, which are proportional to the square of the perpendicular component of the magnetic dipole vector (Fig. 1), should decrease markedly with increasing angular momentum. This behavior cannot be reproduced within the standard Dönau and Frauendorf cranking formalism [9]. The shears picture has been confirmed in the lead region through studies of the behavior of the $B(M1)$ values extracted from lifetime measurements [10,11] and a measurement of the g factor of the bandhead of a magnetic dipole band in ^{193}Pb, which confirmed the initial perpendicular coupling of the component proton and neutron spin vectors [12]. However, it is not clear if the shears mechanism will be active in the light tin region, where the spin vectors are expected to be shorter than in the lead region, due to the lower-j orbitals involved. Furthermore, the nuclei have a small prolate deformation in contrast to the oblate deformation, $\epsilon_2 \approx -0.1$, of the lead nuclei. The behavior of the $B(M1)$ values should provide a discriminating test between the involvement of collective rotation and the shears mechanism in generating these structures in the light tin nuclei.

In the present paper, the Doppler shift attenuation method (DSAM) has been employed in order to obtain lifetimes for states in two $M1$ bands, one in each of the nuclei ^{106,108}Sn. The results have enabled $B(M1)$ transition rates to be deduced which clearly demonstrate the rapid decrease with increasing angular momentum expected from the shears bands. Comparison of these data with previous TAC calculations has highlighted

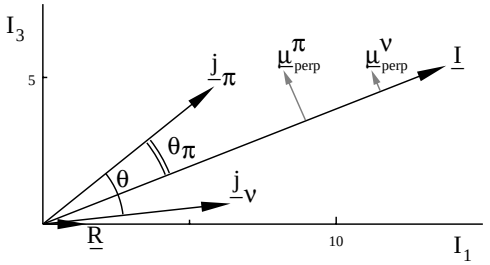

FIG. 1. Illustration of the shears mechanism and the respective angles involved for a typical shears band. $\underline{\mathbf{I}}$ is the total angular momentum, and $\underline{\mathbf{j}}_\pi$ and $\underline{\mathbf{j}}_\nu$ are the proton and neutron component vectors, respectively. $\underline{\mathbf{R}}$ is the core component vector. θ and θ_π are the shears angle and the proton angle, respectively. $\mu^\pi_{\rm perp}$ and $\mu^\nu_{\rm perp}$ are the perpendicular components of the proton and neutron magnetic dipole vectors.

 0031-9007/99/83(3)/500(4)$15.00

some limitations when treating near-spherical nuclei within this model. Experimentally deduced $B(E2)$ values suggest that the nuclei are more spherical than previously thought. In addition, $B(M1)$ values calculated using the alternative phenomenological scheme [7,8] are found to be in good agreement with the experimental $B(M1)$ values for both bands. This Letter therefore provides the first confirmation of the involvement of the shears mechanism in generating these structures in near-spherical tin nuclei.

High-spin states in the nuclei ^{106,108}Sn were populated using the ^{54}Fe(^{58}Ni, $\alpha 2p$) and ^{54}Fe(^{58}Ni, $4p$) reactions, respectively, at a beam energy of 243 MeV. The ^{58}Ni beam was incident on an enriched 600 μg/cm^2 ^{54}Fe target, backed with 15.2 mg/cm^2 of gold. The resulting γ decay was detected by the Gammasphere array [13] containing 95 hyperpure Ge detectors. A total of 2.2×10^9 events of fourfold or higher coincidences were collected. Sufficient statistics were available in order to obtain lifetime information for the more intensely populated of the two bands, band 1 of Ref. [3], in each nucleus. The highfold data were unfolded into triples and sorted into single-gated angle-dependent γ-γ correlation matrices.

Lifetimes were extracted by fitting the Doppler-broadened line shapes using the codes of Wells and Johnson [14]. The slowing down of recoiling nuclei in the target and gold backing was simulated using Monte Carlo methods with 5000 histories and a time step of 0.001 ps, and treated according to the prescription of Gascon *et al.* [15]. The tables of Northcliffe and Schilling [16], with shell corrections, were used for the electronic stopping powers. The histories were used to produce apparent velocity distributions observed by particular angular groups of detectors at an averaged angle based on the geometry of the Gammasphere array. Line shapes were fitted simultaneously to spectra from detectors located at forward (31.7°/37.4°), backward (142.6°/148.3°), and transverse directions with respect to the beam. Fits were carried out assuming a rotational cascade of five transitions, with a moment of inertia of $15\hbar^2$ (MeV)$^{-1}$, feeding into each state, including the topmost state. The side-feeding intensity was estimated from the thick-target data. The side-feeding lifetimes were found to be around a factor of 2 to 3 faster than the in-band lifetimes. In the present paper, the decay scheme for the ^{106}Sn band has been revised [3]. The ordering of the 634 and 780 keV transitions has been reversed and a structure branching at the 20^- level, consisting of the 599 and 571 keV transitions, has been added (see inset of Fig. 3a below). The two permutations of the decay cascade, starting with the 634 and 571 keV transitions, respectively, were fitted independently, yielding consistent lifetimes for the lower three states of the band common to both pathways. The line-shape parameters of the transitions of interest and stopped contaminant peaks were fitted in the spectra for each of the three angles. Typical line-shape fits are shown in Fig. 2. The effective lifetime of the highest state observed was determined and used as an input parameter to a global fit of the entire cascade with variable lifetimes for both in-band and side-feeding states. An error analysis was performed by examining the behavior of the χ^2 value deduced for the fit in the vicinity of the minimum. Quoted errors do not include systematic errors in the stopping powers, which may be as large as 20%. Pure $M1$ character was assumed for the $\Delta I = 1$ transitions when calculating the $B(M1)$ values. The results of this analysis are presented in Table I.

In our previous work, TAC calculations suggested a structure of $\pi[(g_{9/2})^{-1} g_{7/2}] \otimes \nu[h_{11/2}(g_{7/2}, d_{5/2})]$ for band 1 in ^{108}Sn and $\pi[(g_{9/2})^{-1} g_{7/2}] \otimes \nu[h_{11/2}(g_{7/2}, d_{5/2})^3]$ for band 1in ^{106}Sn [3]. These

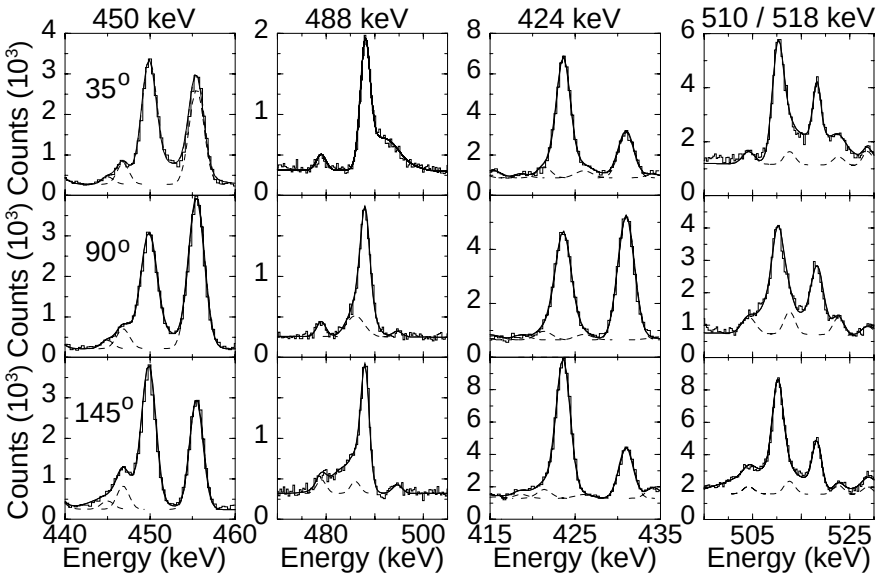

FIG. 2. Representative spectra showing fitted line shapes for the 450 and 488 keV transitions in ^{106}Sn and the 424, 510, and 518 keV transitions in ^{108}Sn. Dashed lines indicate contaminant peaks.

TABLE I. Results of line shape analysis for ^{106}Sn (top) and ^{108}Sn (bottom). τ is the mean lifetime of the state, depopulated by the gamma ray E_γ. Errors in reduced transition ratios, $B(M1)$ and $B(E2)$, are cumulative from errors in branching ratios, $B_\lambda(M1)$, and lifetimes. The shears angle θ and proton angle θ_π are obtained by the methods described in the text.

E_γ (keV)	$B_\lambda(M1)$ (%)	τ (ps)	$B(M1)$ (μ_N^2)	$B(E2)$ (e^2b^2)	θ (°)	θ_π (°)
449.7	>96	$0.30^{+0.03}_{-0.03}$	$2.06^{+0.22}_{-0.26}$	<0.011	78.9	64.5
488.1	>98	$0.43^{+0.05}_{-0.05}$	$1.12^{+0.15}_{-0.13}$	<0.004	65.4	52.8
591.9	>98	$0.51^{+0.15}_{-0.15}$	$0.54^{+0.20}_{-0.13}$	<0.002	49.2	39.2
599.3	86(5)	$0.22^{+0.04}_{-0.05}$	$1.14^{+0.26}_{-0.22}$	$0.021^{+0.008}_{-0.009}$	79.0	66.7
780.4	>96	$0.22^{+0.05}_{-0.06}$	$0.54^{+0.15}_{-0.12}$	<0.003	25.3	19.9
423.7	95(1)	$0.66^{+0.06}_{-0.06}$	$1.05^{+0.10}_{-0.10}$	$0.035^{+0.004}_{-0.005}$	45.4	32.7
509.9	86(2)	$0.23^{+0.02}_{-0.02}$	$1.63^{+0.11}_{-0.11}$	$0.070^{+0.012}_{-0.010}$	78.9	62.7
518.2	82(2)	$0.29^{+0.04}_{-0.02}$	$1.16^{+0.07}_{-0.16}$	$0.045^{+0.006}_{-0.008}$	64.9	50.8
535.1	77(3)	$0.44^{+0.06}_{-0.04}$	$0.64^{+0.10}_{-0.09}$	$0.033^{+0.007}_{-0.006}$	48.0	37.1
550.2	79(3)	$0.56^{+0.13}_{-0.13}$	$0.48^{+0.11}_{-0.11}$	$0.021^{+0.006}_{-0.005}$	22.0	16.8

calculations successfully reproduced some of the experimental features such as the observed $B(M1)/B(E2)$ ratios in ^{108}Sn. However, $B(M1)$ values, predicted as a by-product of this analysis (unpublished), do not decrease as rapidly with increasing spin as the experimental values, indicating that the calculated deformations used previously may be too great. The TAC calculations are sensitive to the strength of the coupling constant of the quadrupole-quadrupole (Q-Q) interaction. Previously, this was chosen such that it reproduced the deformation obtained by means of Strutinsky's shell correction method. Such a procedure is appropriate for substantial deformations but may not be so for near-spherical nuclei. Lifetimes obtained in the present paper have allowed $B(M1)$ and $B(E2)$ values (or limits) to be determined for the $M1$ bands in ^{106,108}Sn. These data indicate that a reduction in the Q-Q coupling constant of about 10% is necessary in order to reproduce the experimental $B(E2)$ values. This adjustment yielded deformations of $\epsilon_2 = 0.08$ and $\epsilon_2 = 0.11$ for the ^{108}Sn band, before and after the $g_{7/2}$ neutron alignment at $I \sim 16\hbar$, respectively, which are somewhat smaller than the value, $\epsilon_2 = 0.14$, obtained from the Strutinsky procedure. A similar adjustment for ^{106}Sn suggests that a deformation of $\epsilon_2 = 0.03$ is more appropriate than the value, $\epsilon_2 = 0.11$, obtained from the Strutinsky method.

The $B(M1)$ values calculated for both nuclei, using the TAC model with the new deformations, show improved agreement with the experimental $B(M1)$ values (see Fig. 3) over the previous calculations, which predicted a much flatter $B(M1)$ curve with increasing spin. The remaining difference between theory and experiment can probably be attributed to the deformation being treated as a constant within the TAC model, for a given configuration. This is a severe limitation since the $B(E2)$ values, and hence the collectivity, clearly decrease with increasing spin for a fixed configuration (see Table I).

The 21^- state, depopulated by the 599 keV gamma ray, in ^{106}Sn has an associated $B(M1)$ value of $1.14\mu_N^2$. This is consistent with the alignment of a pair of $h_{11/2}$ neutrons occurring at a frequency of $\sim$0.6 MeV/$\hbar$.

A semiclassical derivation of $B(M1)$ values in terms of the coupling scheme, illustrated in Fig. 1, has been attempted [7,8]. The $B(M1)$ values are derived in terms of the angle θ_π, which the proton spin vector makes with the total vector $\underline{\mathbf{I}}$. It is found that $B(M1) = \frac{3}{8\pi}\, g_{\rm eff}^2 j_\pi^2 \sin^2\theta_\pi$, where $g_{\rm eff}$ is the difference between the proton and neutron g factors [7].

If it is assumed that the proton spin vector originates from the $g_{9/2}$ proton hole, i.e., $|\mathbf{j}_\pi| = 4.5\hbar$, and that at the bandhead the proton and neutron vector coupling is perpendicular; the length of the remaining vector $\underline{\mathbf{j}}_\nu$ is then fixed since the length of the total angular momentum vector $\underline{\mathbf{I}}$ equals the spin of the bandhead. Higher spin values are obtained by closing the shears. Using the relationship given above, $B(M1)$ transition rates have been determined for the respective bands using values of $g_{\rm eff}$ obtained from empirical g factors for this region [17,18]. The g factors were combined by means of the additivity formula of Ref. [19]. For the ^{108}Sn band, it is found that an effective g factor of 1.11 is appropriate for the $\pi[(g_{9/2})^{-1}g_{7/2}] \otimes \nu[h_{11/2}g_{7/2}]$ configuration. The maximum spin which may be generated from this fixed geometry is $\sim 15\hbar$. Around this spin, the alignment of a pair of $g_{7/2}$ neutrons is observed [3] leading to the $\pi[(g_{9/2})^{-1}g_{7/2}] \otimes \nu[h_{11/2}(g_{7/2})^3]$ configuration, for which an effective g factor of 0.94 is obtained using the additivity formula and a measured value for the aligned pair of neutrons of $g[(\nu g_{7/2})^2_{6+}] = 0.43$ [20]. Similar calculations have been performed for the band in ^{106}Sn. In this case, a bandhead spin of $17\hbar$ was assumed and an effective g factor of 0.94 was adopted for the previously suggested [3] $\pi[(g_{9/2})^{-1}g_{7/2}] \otimes \nu[h_{11/2}(g_{7/2})^3]$ configuration. The values of the shears angle θ and proton angle θ_π used in the calculations are given in Table I,

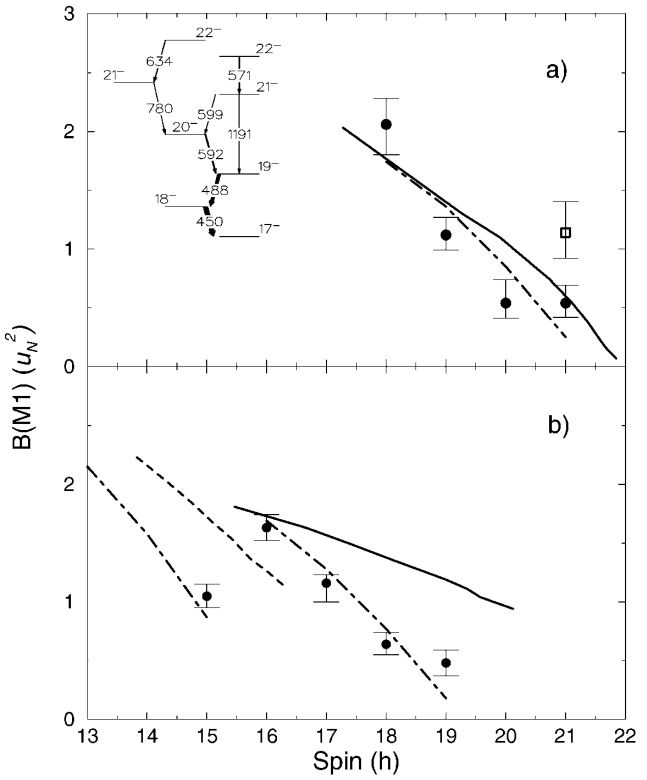

FIG. 3. (a) Plot of $B(M1)$ values against spin for ^{106}Sn. The solid line represents a TAC calculation for the configuration discussed in the text. The open square results from the branch (see text) thought to arise from the alignment of an $h_{11/2}$ neutron pair. The inset shows the ^{106}Sn $M1$ band. (b) Plot of $B(M1)$ values against spin for ^{108}Sn. The dashed and solid lines represent the results of TAC calculations using configurations [below (dashed line) and above (solid line) the $\nu g_{7/2}$ alignment] described in the text. The dotted-dashed lines in both (a) and (b) show the predictions of the phenomenological model using effective g factors appropriate to the configurations described in the text.

and the predicted $B(M1)$ values are compared with experimental values in Fig. 3. The excellent agreement for both nuclei provides good evidence for the near perpendicular coupling of the proton and neutron configurations at the bandhead. Furthermore, the results imply a very low core contribution to the total angular momentum and the angular momentum is almost entirely generated by the shears mechanism.

Systematic error enters the above semiclassical analysis through the assumption of the location of the bandhead and of the initial perpendicular coupling of the component vectors, which, if less than 90°, would reduce the calculated $B(M1)$ values. Furthermore, the contribution to the total spin from the weakly deformed rotating core is ignored. This assumption may be justified by the very low deformations indicated by the measured $B(E2)$ values.

In conclusion, lifetimes of states of an $M1$ band in each of the nuclei ^{106,108}Sn have been obtained by means of the DSAM technique. Derived $B(M1)$ values exhibit a rapid decrease with increasing spin, demonstrating, for the first time, that the shears mechanism generates the majority of the angular momentum in such structures in the light tin nuclei. The results yield a very low collectivity for these structures and qualitatively verify the perpendicular coupling of the assigned configurations from derived effective g factors. Similar structures in the lead region have an oblate deformation of $\epsilon_2 \approx -0.1$, whereas this paper clearly demonstrates that the deformation involved in these magnetic rotational structures in the tin nuclei is negligible; indeed, the band in ^{106}Sn appears to be the first example of almost pure magnetic rotation.

The authors thank the staff of the LBNL 88-Inch Cyclotron, A. Lipski for making the targets, and John Wells for providing the latest line shape analysis package. This work was supported in part by the U.S. NSF and DOE under Contract No. DE-AC03–76SF00098, the UK EPSRC, AECL, and the Canadian NSERC.

*Present address: Dept. of Physics, University of Liverpool, Liverpool L69 7ZE, U.K.
†Physics Department, Yale University, New Haven, CT 06520.
‡Present address: Lawrence Berkeley National Laboratory, Berkeley, California 94720.
§Present address: Schuster Laboratory, University of Manchester, Manchester M13 9PL, U.K..
‖Present address: Dept. of Physics, University of Notre Dame, Notre Dame, IN 46556.

[1] G. Baldsiefen *et al.*, Nucl. Phys. **A574**, 521 (1994).
[2] A. Gadea *et al.*, Phys. Rev. C **55**, 1 (1997).
[3] D. G. Jenkins *et al.*, Phys. Lett. B **428**, 23 (1998).
[4] S. Frauendorf, J. Meng, and J. Reif, in *Proceedings of the Conference on Physics from Large γ Ray Detectors, Berkeley, 1994*, (internally published by LBNL, 1995), Vol. II, p. 52 (Report No. LBL-35687), available from National Technical Information Service, U.S. Dept. of Commerce, Springfield, Va. 22161.
[5] S. Frauendorf, Nucl. Phys. **A557**, 259c (1993).
[6] S. Frauendorf, in *Proceedings of Workshop on Gammasphere Physics, Berkeley, 1995* (World Scientific, Singapore, 1996), p. 272.
[7] A. O. Macchiavelli *et al.*, Phys. Rev. C **57**, R1073 (1998).
[8] A. O. Macchiavelli *et al.*, Phys. Rev. C **58**, R621 (1998).
[9] F. Dönau and S. Frauendorf, in *Proceedings of the International Conference on High Angular Momentum properties of Nuclei, Oak Ridge* (Harwood, Chur, Switzerland, 1983), p. 143.
[10] R. Krücken *et al.*, Phys. Rev. C **58**, R1876 (1998).
[11] R. M. Clark *et al.*, Phys. Lett. B **440**, 251 (1998).
[12] S. Chmel *et al.*, Phys. Rev. Lett. **79**, 2002 (1997).
[13] I. Y. Lee, Nucl. Phys. **A520**, 641c (1990).
[14] J. C. Wells and N. Johnson (private communication).
[15] J. Gascon *et al.*, Nucl. Phys. **A513**, 344 (1990).
[16] L. C. Northcliffe and R. F. Schilling, Nucl. Data Tables **7**, 233 (1970).
[17] T. Lonnröth, S. Vadja, O. C. Kistner, and M. H. Rafailovich, Z. Phys. A **317**, 215 (1984).
[18] P. van Nes *et al.*, Z. Phys. A **301**, 137 (1981).
[19] H. Hübel, Fortschr. Phys. **25**, 481 (1977).
[20] A. Makishima *et al.*, Z. Phys. A **349**, 133 (1994).